Attributing intensification of precipitation extremes to human influence

Xuebin Zhang,[1] Hui Wan,[1] Francis W. Zwiers,[2] Gabriele C. Hegerl,[3] and Seung-Ki Min[4]

Received 15 August 2013; revised 27 September 2013; accepted 29 September 2013; published 11 October 2013.

[1] This study provides estimates of the human contribution to the observed widespread intensification of precipitation extremes. We consider the annual maxima of daily (RX1day) and 5 day consecutive (RX5day) precipitation amounts over the Northern Hemisphere land area for 1951–2005 and compare observed changes with expected responses to external forcings as simulated by multiple coupled climate models participating in Coupled Model Intercomparison Project Phase 5. The effect of anthropogenic forcings can be detected in extreme precipitation observations, both individually and when simultaneously estimating anthropogenic and naturally forced changes. The effect of natural forcings is not detectable. We estimate that human influence has intensified annual maximum 1 day precipitation in sampled Northern Hemisphere locations by 3.3% [1.1% to 5.8%, >90% confidence interval] on average. This corresponds to an average intensification in RX1day of 5.2% [1.3%, 9.3%] per degree increase in observed global mean surface temperature consistent with the Clausius-Clapeyron relationship. **Citation:** Zhang, X., H. Wan, F. W. Zwiers, G. C. Hegerl, and S.-K. Min (2013), Attributing intensification of precipitation extremes to human influence, *Geophys. Res. Lett.*, *40*, 5252–5257, doi:10.1002/grl.51010.

1. Introduction

[2] Atmospheric saturation vapor pressure increases as temperature increases according to the Clausius-Clapeyron relationship. As relative humidity is not expected to change much [*Allen and Ingram*, 2002], global warming would result in increased atmospheric moisture content. Consequently, extreme precipitation will increase since extreme precipitation is mainly constrained by the availability of moisture [*Allen and Ingram*, 2002]. Evidence suggests that anthropogenic influence has changed the spatial distribution of precipitation over global land areas [*Zhang et al*., 2007; *Polson et al*., 2013], increased high-latitude precipitation [*Min et al*., 2008], and increased atmospheric moisture content [*Santer et al*., 2007; *Willett et al*., 2007].

[3] Rainfall observations show that extreme precipitation over land has intensified on average [*Groisman et al*., 2005; *Alexander et al*., 2006; *Trenberth et al*., 2007; *Donat et al*., 2013; *Westra et al*., 2013]. Human induced global warming may be a contributing factor. *Westra et al*. [2013] showed that the observed increase in annual maximum 1 day precipitation per degree surface temperature increase is at a rate (5.9% K^{-1} to 7.7% K^{-1}) close to that which would be expected from the Clausius-Clapeyron relationship (~7% K^{-1}). In a recent study [*Min et al*., 2011], we linked the observed intensification of precipitation extremes to human influence using simulations from a limited set of coupled climate models (GCMs) participating in the Coupled Model Intercomparison Project Phase III (CMIP3) and observations with limited spatial coverage ending in year 2000. Based on these data, detection of the response to all external forcings including both anthropogenic and natural forcings was less robust than detection of the response to anthropogenic forcing alone. Also, the GCMs showed substantially smaller changes than observed [*Min et al*., 2011].

[4] Here we use a newly updated observational data set with both improved spatial and temporal coverage [*Donat et al*., 2013]. We further improved spatial coverage by augmenting this data set with newly available Russian data (http://www.meteo.ru/English/climate/d_temp.php). We analyze observed changes using multimodel ensemble GCM simulations available from the Coupled Model Intercomparison Project Phase 5 (CMIP5) to quantify human influence on annual extreme precipitation. The remainder of the paper is structured as follows: We describe observed and simulated data in section 2, methods and data processing are detailed in section 3, and the main results are presented in section 4. We conclude the paper with conclusions and discussion in section 5.

2. Data

[5] We used the annual maxima of daily (RX1day) and 5 day consecutive (RX5day) precipitation amounts for 1951–2005 from the HadEX2 data set [*Donat et al*., 2013]. Spatial coverage of observational data is lower outside this period, and historical climate simulations extending past 2005 are available from only a few GCMs. RX1day and RX5day are frequently used indices of extreme precipitation in flood risk assessments [*Bates et al*., 2008; *Seneviratne et al*., 2012] and were used in the analysis of observed changes in extreme precipitation [*Alexander et al*., 2006; *Donat et al*., 2013] and in our previous study of human influence on precipitation extremes [*Min et al*., 2011]. HadEX2 is a gridded (2.5° × 3.75° latitude-longitude) land-based data set of indices of temperature and precipitation extremes [*Donat et al*., 2013] that updates the HadEX data set [*Alexander et al*., 2006] with improved spatial and temporal coverage. Nevertheless, HadEX2 coverage of Russia is limited after the late 1990s. We therefore augment HadEX2 with

Additional supporting information may be found in the online version of this article.

[1]Climate Research Division, Environment Canada, Toronto, Ontario, Canada.
[2]Pacific Climate Impacts Consortium, University of Victoria, Victoria, British Columbia, Canada.
[3]School of GeoSciences, University of Edinburgh, Edinburgh, UK.
[4]School of Environmental Science and Engineering, Pohang University of Science and Technology, Pohang, South Korea.

Corresponding author: X. Zhang, Climate Research Division, Environment Canada, Toronto, Ontario M3H 5T4, Canada. (Xuebin.Zhang@ec.gc.ca)

0094-8276/13/10.1002/grl.51010

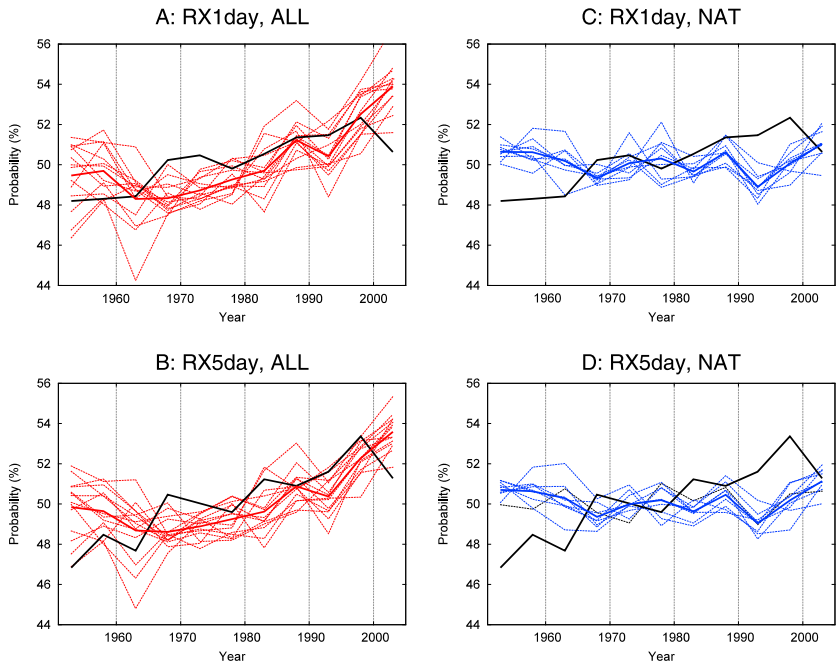

Figure 1. Time series of 5 year mean area-averaged PI over Northern Hemisphere land during 1951–2005. (a and b) Model simulations with anthropogenic plus natural external (ALL) forcing (54 runs from 14 GCMs); (c and d) model simulations with natural external (NAT) forcing (34 runs from 9 GCMs). For each pair of panels, results are shown for RX1day and RX5day. Black lines are observations. Red (ALL) and blue (NAT) solid lines represent multimodel means. Red (ALL) and blue (NAT) dashed lines indicate results for individual model averages.

newly available daily precipitation observations from more than 600 Russian Met Service stations (section 3.1).

[6] Multimodel simulations were obtained from the CMIP5 archive (supporting information Table S1). RX1day and RX5day indices for GCMs were calculated following *Sillmann et al.* [2013]. Indices were available from 54 simulations driven with historical anthropogenic plus natural forcing (ALL) from 14 GCMs at the time of analysis, and 34 driven with historical natural forcing (NAT) from 9 GCMs (see supporting information Table S1). Most GCM simulations end in 2005. Analyses were conducted using ALL and NAT signal estimates from all available GCMs, and from the subset of 7 GCMs with both ALL and NAT simulations. We also used >15,000 years of unforced control simulations (CTL) from 31 GCMs (supporting information Table S1). In total, we used 460 fifty-five year chunks of model output for the estimation of natural variability.

3. Methods and Data Processing

3.1. Data Processing

[7] The GCMs project increases in extreme precipitation globally except in some subtropical regions [*Sillmann et al.*, 2013; *Kharin et al.*, 2013]. Observational data are lacking in these subtropical regions. As a result, the expected signal in extreme precipitation shows increases over all regions where observational data are available for detection and attribution analysis (see also *Hegerl et al.*, 2004 and supporting information Figure S5). This, together with low signal-to-noise ratios in extreme precipitation (e.g., *Westra et al.*, 2013) suggests that large-area averaging of extreme precipitation indices may reduce noise and improve the likelihood of detecting the responses to external forcing.

[8] The magnitude of precipitation is highly variable from one region to another. Hence, the temporal variability of spatial averages of RX1day and RX5day observations is dominated by variability from areas with large precipitation amounts. Further, changes in data availability with time may introduce inhomogeneities into time series of spatial averages [*Wan et al.*, 2013]. To reduce these effects and improve representativeness and intercomparability, we standardized HadEX2 values at each grid box by transforming the data into an index based on probability (PI) [*Min et al.*, 2011]. PI is obtained by fitting generalized extreme value (GEV) distributions to RX1day and RX5day at individual grid points, and using the fitted distributions to convert precipitation amounts into a probability scale between 0 and 1. Using an empirical estimate of PI based only on the rank of observed precipitation amounts produces virtually identical regional averages (Figure S4). Grid box values based on Russian station data are obtained by averaging RX1day and RX5day station data within individual 2.5° × 3.75° grid boxes and then converting to PI as well. The gridded Russian PI data replace corresponding PI values from HadEX2. The resulting merged data set has improved spatial and temporal coverage over eastern Eurasia and is robust to processing choices (supporting information, section S1).

[9] Since GCM simulated RX1day and RX5day values have different spatial resolutions in different GCMs, they are interpolated to the HadEX2 grid using inverse distance weighted averages of the four nearest grid box values. In contrast to *Min et al.* [2011], this interpolation is done before model data are converted to PI. The interpolated GCM data for 1951–2005 are masked to mimic the availability of observational data and then converted to PI; masking ensures that observations and GCMs are similarly affected by data availability in the conversion to PI and subsequent spatial averaging (supporting information, section S2).

[10] We consider only Northern Hemisphere land areas since observational data are limited in the Southern Hemisphere. Supporting information, Figure S1 shows the spatial coverage of data used in the analysis. We calculate nonoverlapping 5 year mean PI averaged over land in the Northern Hemisphere (NH), two broad zonal NH regions including the midlatitudes (30°–65°N, ML) and the tropics and subtropics (0°–30°N, TR), and three NH west-east regions including the western NH (50°W–180°W, NA), western Eurasia (15°W–60°E, EU), and eastern Eurasia (60°E–180°E, AS). Only grid boxes with 45 or more years of data over 1951–2005 are used (supporting information, section S1).

[11] Figure 1 shows the time evolution of the NH 5 year PI means. Observed PIs have upward trends, indicating intensification of both 1 day and 5 day precipitation extremes. The multimodel PI mean of ALL simulations shows a similar trend for both RX1day and RX5day, though values in the 1960s are slightly lower than the 1950s. The multimodel PI mean of NAT simulations does not exhibit a trend. Observed PIs are within the range of individual model ALL simulations, but not within those of NAT simulations (Figure 1). The updated observational data show slightly reduced trends compared to *Min et al*. [2011], particularly for RX1day PI. This is due to smaller trends in Russian data and slightly less intense precipitation extremes in recent years (Figure 1 and supporting information Figure S3).

3.2. Detection Method

[12] A frequently used method for detection and attribution analysis is the optimal fingerprint detection method in which observations $\boldsymbol{y}$ (PI) are regressed via generalized total least squares [*Allen and Stott*, 2003] onto model simulated signals $\mathbf{X}$ (a matrix with one column for each signal considered) such that $\boldsymbol{y} = \mathbf{X}\beta + \varepsilon$. Detection is claimed when the scaling factors $\boldsymbol{\beta}$ are significantly greater than zero. Both observations and signals are centered on zero by subtracting the expected mean PI value 0.5 when conducting the regression analysis. Signals are estimated by averaging PI from individual model ensemble PI means in the same forcing group for 1951–2005.

[13] We use the total least square (TLS) method to conduct detection analyses, both with [*Allen and Stott*, 2003] and without [*Polson et al*., 2013] using optimal fingerprints (also referred to prewhitening the data;[*Allen and Stott*, 2003]) on individual regional PI averages for NH, ML, TR, NA, EU, AS, and for the NH in either two or three regions combining ML and TR averages or NA, EU, and AS averages, respectively. When multiple regions are used in the analysis, data are weighted by the area of the available data grid boxes within each region. We estimate the anthropogenic forced signal (ANT) as the difference between ALL and NAT under the assumption of linearly additive responses to the external forcings. The optimal analysis requires two independent estimates of the internal variability covariance structure for optimization and uncertainty analysis [*Hegerl et al*., 1997], which are estimated from interensemble variability and preindustrial control simulations (supporting information section S2). The uncertainty in the scaling factors from the nonoptimized analyses is estimated using the bootstrap procedure of *Polson et al*. [2013] (supporting information section S3).

[14] We conduct single-signal analyses by regressing observations onto model simulated extreme precipitation responses to ALL, ANT, and NAT forcings estimated from the relevant multimodel ensemble averages. We found a substantial correlation between annual series of ALL and NAT (correlation coefficient 0.34) but not between ANT and NAT (correlation coefficient −0.16). We conducted a two-signal optimal detection and attribution analysis in which observations are regressed onto ANT and NAT signals simultaneously, in order to estimate the contribution by both natural and anthropogenic forcings to changes in extreme precipitation. Regressing the observed PI onto ANT and NAT rather than ALL and NAT removes colinearity between the signals. Our analysis accounts for the fact that the ANT signal estimate is affected by noise that is present in both the ALL and NAT signal estimates. Results are robust to using either ALL or ANT in combination with NAT (supporting information section S4).

[15] The influence of external forcing is detected by determining whether the amplitudes (scaling factors) of model signals are significantly greater than zero. Consistency between observed and simulated changes is assessed by determining whether the scaling factors are not significantly different from unity. As model simulated internal variability is used to estimate scaling factor uncertainty, model simulated variability is compared to the regression residuals with a residual consistency test [*Allen and Stott*, 2003; *Ribes and Terray*, 2013].

4. Results

4.1. Single-Signal Analyses

[16] Figure 2 shows scaling factor best estimates for ALL, ANT, and NAT based on single-signal optimal analyses. The scaling factors for ALL and ANT are significantly greater than zero for both RX1day and RX5day in analyses with one (NH), two (midlatitude and northern tropics combined, ML + TR), and three (North America, Europe, Asia combined, NA + EU + AS) NH land regions, indicating that the combined effect of external anthropogenic and natural forcing or the effect of anthropogenic forcing alone can be detected in extreme precipitation over Northern Hemispheric land. The 90% uncertainty ranges include unity, indicating that the model simulated changes in extremes transformed to PI under ALL and ANT forcing are consistent with the change in observations. This differs from *Min et al*. [2011] in which the GCMs seemed to have underestimated the observed change. Multiple factors including larger spatial coverage, larger data sets for the estimation of signals and natural variability seem to have contributed to this improvement, although a detailed discussion is beyond the scope of this paper.

[17] The scaling factors for the NAT-only signal are smaller than zero, and in some cases significantly less than zero (Figure 2). This could be due to several reasons. Regressing the observations onto signals with low signal-to-noise ratios via total least squares may distort the signals and produce nonphysical signal amplitudes [*Ribes and Terray*, 2013]. Additionally, from a regression model selection point of view, a lack of the inclusion of predictors representing the primary components of external forcing such as ANT may have rendered the NAT-only regression model invalid.

[18] The scaling factors for ALL and ANT are also significantly greater than zero for the ML, NA, and EU regions, indicating that influence of external forcing on extreme precipitation is also detectable on continental scales. However,

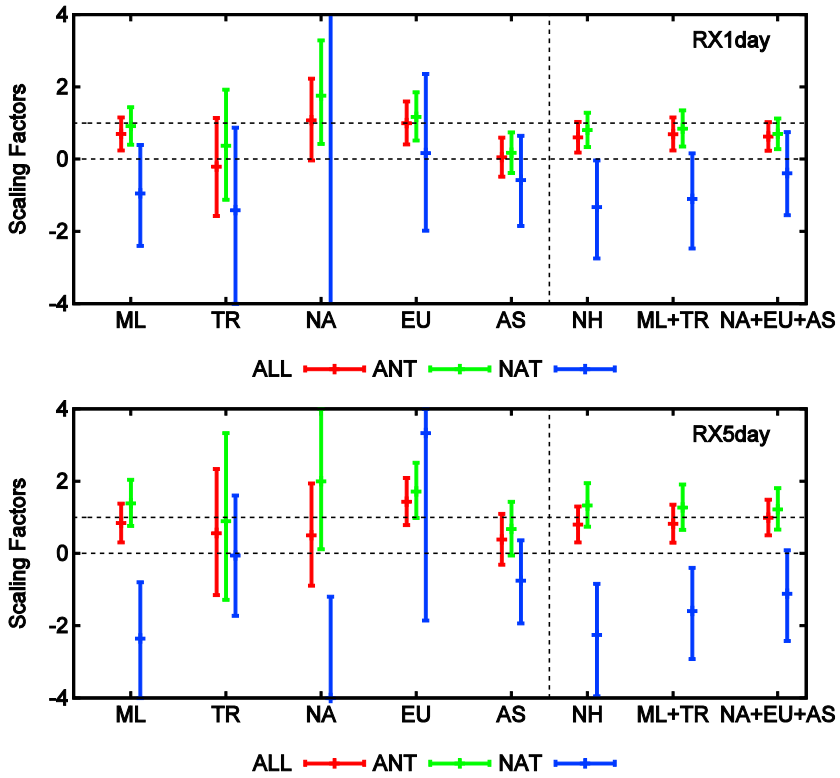

Figure 2. Results from single-signal optimal detection analyses of extreme precipitation indices for (top) RX1day and (bottom) RX5day. Best estimates (data points) and 5–95% confidence intervals (error bars) of the scaling factors are displayed for ALL, ANT, and NAT, when using 5 year mean PI averaged over midlatitude (ML), northern tropics (TR), western Hemisphere land (NA), western East Hemisphere land (EU), and eastern East Hemisphere land (AS), Northern Hemisphere (NH), and when using two regional averages (ML + TR) or three regional averages (NA + EU + AS). Refer to supporting information Figure S6 for results from nonoptimized detection analyses.

detection becomes more difficult for the regions overall. Single-signal nonoptimized analyses show essentially the same results, indicating that nonoptimized analyses produce robust results in this case, although scaling factor estimates are in general associated with larger uncertainty bands when the signal strength is strong (e.g., ALL, ANT, and Figure S6) than those resulting from optimal detection.

4.2. Two-Signal Optimal Fingerprint Analysis

[19] Figure 3 shows the best estimate scaling factors for ANT and NAT in two-signal analyses of Northern Hemisphere land in three regions (NA + EU + AS), together with their marginal confidence intervals and joint confidence regions. Even when separately estimating the naturally forced signal, the anthropogenic influence is detected at the 10% significance level in both RX1day and RX5day. The ANT scaling factors are significantly greater than zero and consistent with one in both cases. The NAT scaling factors are not significantly different from zero. This indicates that the simulated ANT response is consistent with observed changes while the simulated NAT response is not significantly contributing to observed changes. The two-signal analyses conducted in one or two regions (NH or ML + TR, and supporting information Figure S13), and with ANT and NAT simulated by the same GCMs, yield similar results (supporting information Figure S12).

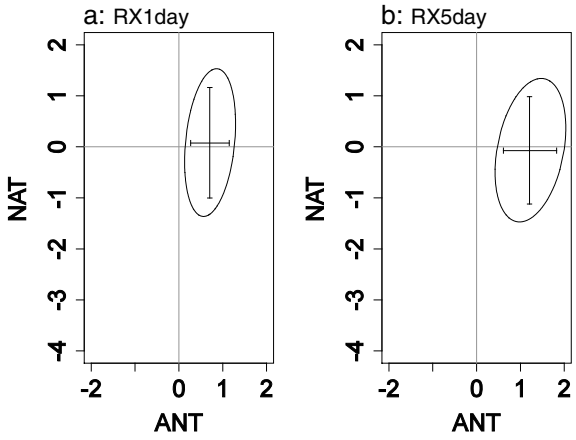

Figure 3. Results from two-signal optimal detection analyses of extreme precipitation indices. for (a) RX1day and (b) RX5day when using 5 year mean PI in three (NA + EU + AS) regional averages combined with weighting to NA, EU, and AS corresponding to areas of available data grids. The intersections of the two error bars represent best estimates of the scaling factors for ANT and NAT. The 5–95% marginal confidence intervals of the scaling factors are displayed as error bars. The 5–95% joint confidence regions are represented by ellipses.

[20] Similar conclusions are obtained when the detection and attribution analyses are conducted on spatial averages of nonoverlapping 5 year mean series for 1951–2000, 3 year mean series, or annual PI values for 1951–2005 directly. For annual values in more than one spatial domain, it is no longer possible to produce full rank estimates of internal covariability from the available collection of CMIP5 simulations. Optimal detection analyses are conducted on a reduced space spanned by the leading Empirical Orthogonal Functions (EOFs) of model simulated variability. Detection results are not sensitive to EOF truncation in this case, however (supporting information section S4).

4.3. Estimating Extreme Precipitation Changes Attributable to Anthropogenic Influence

[21] To estimate extreme precipitation changes attributable to anthropogenic influence, we first estimate PI changes attributable to human influence. We assume that the PI response to anthropogenic forcing (ANT) is the difference between model simulated responses to ALL and NAT forcing. Linear trends in ANT in the 5 year nonoverlapping RX1day and RX5day series are estimated to be 5.0% and 3.9%, respectively over the 55 year period. We multiply these ANT trends by the ANT scaling factors and their 90% confidence intervals obtained based on optimized single-signal and two-signal analyses conducted on one-region NH, two-region ML and TR, and three-region NA, EU, and AS series. This results in six sets of ANT attributed PI trend estimates for the RX1day and RX5day series. Results are provided in the supporting information, Table S2. Based on these trends, we estimate the median attributable PI changes δPI to be 4.0% [1.4 to 6.8%] for RX1day and 4.7% [1.9% to 7.5%] for RX5day, where the uncertainty estimates are conservatively constructed by finding the smallest interval that contains the individual 90% confidence intervals.

[22] We convert these attributable PI changes to attributable annual extreme precipitation changes using the following steps: (1) We compute the median value of extreme precipitation (corresponding to PI = 50%) X_{50} for an individual grid box or station. (2) We apply the estimated NH attributable PI changes to individual grid boxes or individual stations implying an assumption that the attributable PI change is the same at all locations. (3) We further assume that changes only occur in the location parameter of the GEV distributions. This is supported by studies of historical trends in extreme precipitation (e.g., *Westra et al*., 2013). (4) We compute two new location parameters μ_1 and μ_0 such that X_{50} has probabilities of (50−δPI/2)/100 and (50+ δPI/2)/100, respectively. (5) The ratio $100(\mu_0 - \mu_1)/\mu_1$ is the percent change in the median of annual extreme precipitation at the location. (6) These percent changes are averaged across the spatial domain to obtain a rough estimate of attributable changes in extreme precipitation over the Northern Hemisphere. The resulting median values of attributable changes in extreme precipitation are estimated to be an increase by 3.3% [1.1% and 5.8%] in the intensity of 1 day wettest extremes (RX1day) and 3.8% [1.5% and 6.2%] in the 5 day wettest (RX5day) precipitation extremes (supporting information Table S2). (7) We compute 20 year return values under the distribution with location parameter μ_0; we then compute the new return period of these return values under the distribution with location parameter μ_1. (8) The difference between 20 years and the average of these return periods provides an estimate of the attributable change in return period for 20 year events due to anthropogenic forcing. The median values of return period in the 2000s for a 1950s 20 year event are 15 years [18 years to 12 years] for RX1day and 14 years [17 years to 11 years] for RX5day (supporting information Table S2).

5. Conclusions and Discussion

[23] We find that the multimodel simulated response to the effects of anthropogenic forcing, or anthropogenic and natural forcing combined, are consistent with observed changes in extreme precipitation on average over Northern Hemisphere land. We also find that the observed hemispheric scale change in extreme precipitation (Figure 1) cannot be explained by either natural internal variability or the response to natural external forcing. The detection results are robust to different methods being used. We estimate the human attributable change in PI over 1951–2005 to be 4.0% [1.4%, 6.8%, >90% confidence interval] for RX1day and 4.7% [1.9%, 7.5%] for RX5day. This implies, on average, that a human induced intensification of annual 1 day and 5 day maximum precipitation in sampled NH locations of 3.3% [1.1%, 5.8%] and 3.8% [1.5%, 6.2%], respectively. This corresponds to an average intensification in RX1day of 5.2% [1.3%, 9.3%] per degree increase in global mean surface temperature and 5.9% [2.1%, 9.9%] in RX5day (we used a best estimate linear trend in global mean surface temperature over 1951–2005 of 0.57°C [0.46°C, 0.72°C] based on HadCRUT4 [*Morice et al*., 2012]). This is consistent with the intensification expected as a consequence of warming via the Clausius-Clapeyron relation [*Boer*, 1993; *Allen and Ingram*, 2002], observational estimates of the relationship between the intensity of precipitation extremes and global mean temperature change [*Westra et al*., 2013], and projected future intensification [*Kharin et al*., 2013].This also translates to more frequent extreme precipitation events of a fixed size: the annual maximum 1 day precipitation that was expected to recur once every 20 years on average in the early 1950s is estimated to have become a 15 year event in the early 2000s with the increased frequency being attributable to human influence (supporting information Table S2).

[24] **Acknowledgments.** We thank Nathan Gillett, John Fyfe, and William Ingram for their constructive comments; and Debbie Polson for methodological discussion. We acknowledge the modeling groups, the Program for Climate Model Diagnosis and Intercomparison (PCMDI) and the World Climate Research Programme's (WCRP's) Working Group on Coupled Modeling for their roles in making available WCRP CMIP5 multimodel data. We thank David Bronaugh for assistance with downloading CMIP5 data and processing it into extreme precipitation indices. G.C.H. was supported by the U.S. Department of Energy's Office of Science. Office of Biological and Environmental Research and the National Oceanic and Atmospheric Administration's Climate Program Office (IDAG group), and by the NERC project PAGODA (NE/I006672/1).

[25] The Editor thanks an anonymous reviewer for his assistance in evaluating this paper.

References

Alexander, L. V., et al. (2006), Global observed changes in daily climate extremes of temperature and precipitation, *J. Geophys. Res.*, *111*, D05109, doi:10.1029/2005JD006290.

Allen, M. R., and W. J. Ingram (2002), Constraints on future changes in climate and the hydrologic cycle, *Nature*, *419*, 224–232.

Allen, M. R., and P. A. Stott (2003), Estimating signal amplitudes in optimal fingerprinting. Part I: Theory, *Clim. Dyn.*, *21*, 477–491.

Bates, B. C., Z. W. Kundzewicz, S. Wu, and J. P. Palutikof (Eds.) (2008), *Climate Change and Water. Technical Paper of the Intergovernmental Panel on Climate Change*, IPCC Secretariat, Geneva, pp. 210.

Boer, G. J. (1993), Climate change and the regulation of the surface moisture and energy budgets, *Clim. Dyn.*, *8*, 225–239.

Donat, M. G., et al. (2013), Updated analyses of temperature and precipitation extreme indices since the beginning of the twentieth century: The HadEX2 dataset, *J. Geophys. Res. Atmos.*, *118*, 2098–2118, doi:10.1002/jgrd.50150.

Groisman, P. Y., R. W. Knight, D. R. Easterling, T. R. Karl, G. C. Hegerl, and V. N. Razuvaev (2005), Trends in intense precipitation in the climate record, *J. Clim.*, *18*, 1326–1350.

Hegerl, G. C., K. Hasselmann, U. Cubasch, J. F. B. Mitchell, E. Roeckner, R. Voss, and J. Waszkewitz (1997), Multi-fingerprint detection and attribution analysis of greenhouse gas, greenhouse gas-plus-aerosol and solar forced climate change, *Clim. Dyn.*, *13*, 613–634.

Hegerl, G. C., F. W. Zwiers, P. A. Stott, and V. V. Kharin (2004), Detectability of anthropogenic changes in annual temperature and precipitation extremes, *J. Clim.*, *17*, 3683–3700.

Kharin, V. V., F. W. Zwiers, X. Zhang, and M. Wehner (2013), Changes in temperature and precipitation extremes in the CMIP5 ensemble, *Clim. Change*, *119*(2), 345–357, doi:10.1007/s10584-013-0705-8.

Min, S.-K., X. Zhang, and F. W. Zwiers (2008), Human-induced Arctic moistening, *Science*, *320*, 518–520.

Min, S. K., X. Zhang, F. W. Zwiers, and G. C. Hegerl (2011), Human contribution to more-intense precipitation extremes, *Nature*, *470*, 378–381.

Morice, C. P., J. J. Kennedy, N. A. Rayner, and P. D. Jones (2012), Quantifying uncertainties in global and regional temperature change using an ensemble of observational estimates: The HadCRUT4 data set, *J. Geophys. Res.*, *117*, D08101, doi:10.1029/2011JD017187.

Polson, D., G. Hegerl, X. Zhang, and T. Osborn (2013), Causes of robust seasonal land precipitation changes, *J. Clim.*, *26*, 6679–6697, doi:10.1175/JCLI-D-12-00474.1.

Ribes, A., and L. Terray (2013), Application of regularised optimal fingerprint to attribution. Part II: Application to global near-surface temperature, *Clim. Dyn.*, doi:10.1007/s00382-013-1736-6.

Santer, B. D., et al. (2007), Identification of human-induced changes in atmospheric moisture content, *Proc. Natl. Acad. Sci. U.S.A.*, *104*, 15,248–15,253, doi:10.1073/pnas.0702872104.

Seneviratne, S. I., et al. (2012), Managing the risks of extreme events and disasters to advance climate change adaptation, in *A Special Report of Working Groups I and II of the Intergovernmental Panel on Climate Change (IPCC)*, edited by C. B. Field, et al., pp. 109–230, Cambridge Univ. Press, Cambridge, U. K.

Sillmann, J., V. V. Kharin, X. Zhang, F. W. Zwiers, and D. Bronaugh (2013), Climate extremes indices in the CMIP5 multimodel ensemble: Part 1. Model evaluation in the present climate, *J. Geophys. Res. Atmos.*, *118*, 1716–1733, doi:10.1002/jgrd.50203.

Trenberth, K. E., et al. (2007), Observations: Atmospheric surface and climate change, in *Climate Change 2007: The Physical Science Basis. Contribution of Working Group I to Fourth Assessment Report of the IPCC*, edited by S. Solomon et al., pp. 235–336, Cambridge Univ. Press, Cambridge, U. K.

Wan, H., X. Zhang, F. W. Zwiers, and H. Shiogama (2013), Effect of data coverage on the estimation of mean and variability of precipitation at global and regional scales, *J. Geophys. Res. Atmos.*, *118*, 534–546, doi:10.1002/jgrd.50118.

Westra, S., L. V. Alexander, and F. W. Zwiers (2013), Global increasing trends in annual maximum daily precipitation, *J. Clim.*, *26*, 3904–3918, doi:10.1175/JCLI-D-12-00502.1.

Willett, K. M., N. P. Gillett, P. D. Jones, and P. W. Thorne (2007), Attribution of observed surface humidity changes to human influence, *Nature*, *449*, 710–712.

Zhang, X., F. W. Zwiers, G. C. Hegerl, F. H. Lambert, N. P. Gillett, S. Solomon, P. Stott, and T. Nozawa (2007), Detection of human influence on 20th century precipitation trends, *Nature*, *448*, 461–465.